Supporting Information

Wireless gas sensing system enabling real-time seafood freshness monitoring based on Ru-In_2O_3 microtubes with dual-enhanced sensitivity and selectivity

Xue-Zhi Song*[,a], Yuxiang Chen,[a] Jintao Zhao,[a] Dekun Liu,[a] Ziwei Lv,[a] Yueying Wang,[a] Zhaonan Zuo,[a] Yu-Lan Meng,[a] Fei Li*[,b], Xiao-Feng Wang*[,a] and Zhenquan Tan*[,a]

[1]School of Chemical Engineering, Ocean and Life Sciences, School of General Education, Leicester International Institute, State Key Laboratory of Fine Chemicals, Dalian University of Technology, 2 Dagong Road, Liaodongwan New District, Panjin, Liaoning 124221, China

2 Medical Oncology Department of Thoracic Tumors, Liaoning Cancer Hospital & Institute, Cancer Hospital of Dalian University of Technology, Shenyang 110042, Liaoning, China

e-mail:

songxz@dlut.edu.cn

wangxf@dlut.edu.cn

tanzq@dlut.edu.cn

lifei@cancerhosp-ln-cmu.com

EXPERIMENTAL SECTION

Chemicals and Materials.

All chemicals, such as indium(III) nitrate tetrahydrate ($In(NO_3)_3 \cdot 4H_2O$), ruthenium(III) chloride hydrate ($RuCl_3 \cdot xH_2O$), 1,4-terephthalic acid (H_2BDC), N,N-dimethyl formamide (DMF, 99.5%), were utilized without undergoing additional purification.

Characterizations.

The analyses were performed using an FEI Nova Nano SEM 450 field emission scanning electron microscope operated at an accelerating voltage of 18 kV. To characterize the crystalline properties of the powder samples, X-ray diffraction (XRD) was conducted using a Shimadzu XRD-7000S diffractometer equipped with a Cu-Kα radiation source (λ = 1.5406 Å) with the scanning speed of 5° min^{-1}. For microscopic characterization, transmission electron microscopy (TEM) and selected area electron diffraction (SAED) patterns were obtained using a Tecnai G2F30 STWIN transmission electron microscope from the United States. The surface chemical composition and valence band spectra were investigated via X-ray photoelectron spectroscopy (XPS) on an ESCALABTM 250Xi spectrometer with an Al Kα radiation source. During the XPS data fitting process, a consistent Lorentz-Gaussian ratio of 80:20 was applied, and the C 1s peak was calibrated to 284.8 eV. The specific area and pore diameter distributions were estimated based on N_2 adsorption isotherm at 77 K. The ultraviolet-visible-near-infrared absorption spectra were collected on a spectrophotometer (Lambda 950, Perkin Elmer).

Fabrication of the smart TEA sensor

In this work, the smart TEA sensing system based on STM32F103C8T6 microcontroller was utilized to assess the gas sensing performance. The analog signal of the dynamic change of the resistance (R_S) of the sensing material caused by gas concentration was converted into a digital signal through the Analog-to-Digital Converter (ADC), and the digital signal was the voltage data (V_{RL}) collected by the ADC. The resistance data (R_S) of the sensing material was calculated by the equation (1):

$$R_s = (V_C/(V_{RL} - 1)) \times R_L \#(Equation\ 1)$$

Forty samples are collected to calculate the average value of the current data every two second, which would avoid the impact of high-frequency noise in the circuit on the experimental data. By the serial communication, the dynamic resistance change data of the sensing material is sent to the ESP32 module in real time for processing and uploading.

A two-minute countdown brings the sensing material to the working temperature. Taking the resistance of the sensing material in clean air as the baseline resistance (R_{air}) and the stable resistance of the sensing material at the target gas concentration as R_{gas}. The sensing response (S) is defined as shown in equation (2):

$$S = R_{air}/R_{gas} \#(Equation\ 2)$$

The sensing response and the target gas concentrations are displayed on the web page in the form of a line graph.

Note S1:

Conversion from the UV-Visible absorption spectra illustrated in **Fig. S13** to the Tauc-plot spectra was performed using the following equation:

$$(\alpha h\nu)^{1/n} = A(h\nu - E_g) \#(Equation\ 3)$$

Where α represents the absorption coefficient, h denotes Planck's constant, signifies a constant, ν represents the photon frequency, A is a constant, E_g represents the band gap, and n is a constant related to the type of semiconductor, which equals 1/2 for In_2O_3.

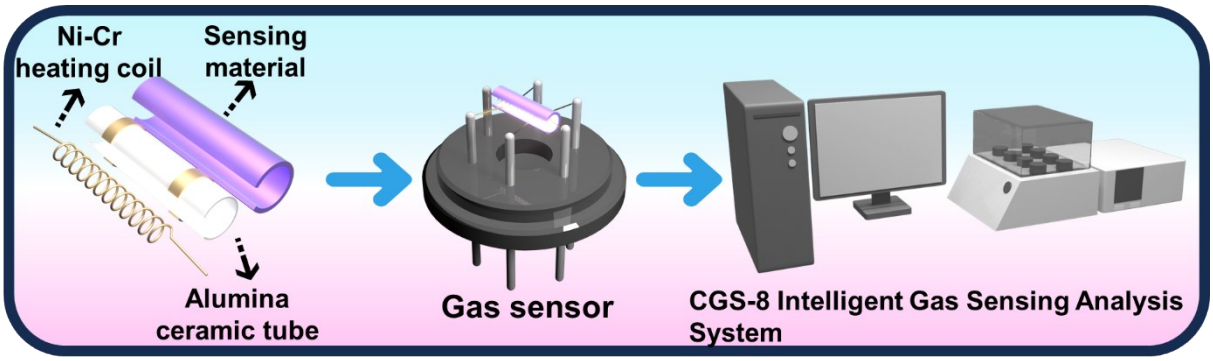

Fig. S1. Schematic of the fabrication of sensor, and the testing instrument

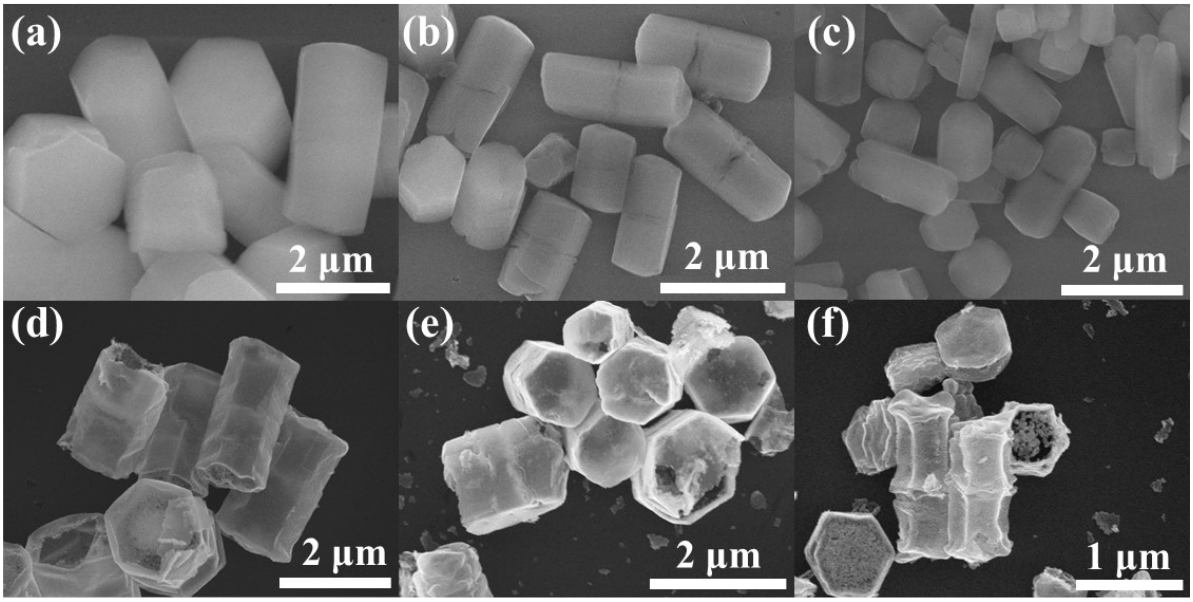

Fig. S2. SEM images of (a) MIL-68, (b) Ru(0.4%)-MIL-68, (c) Ru(1.6%)-MIL-68, (d) pristine In_2O_3, (e)Ru-In_2O_3-0.4, (f)Ru-In_2O_3-1.6

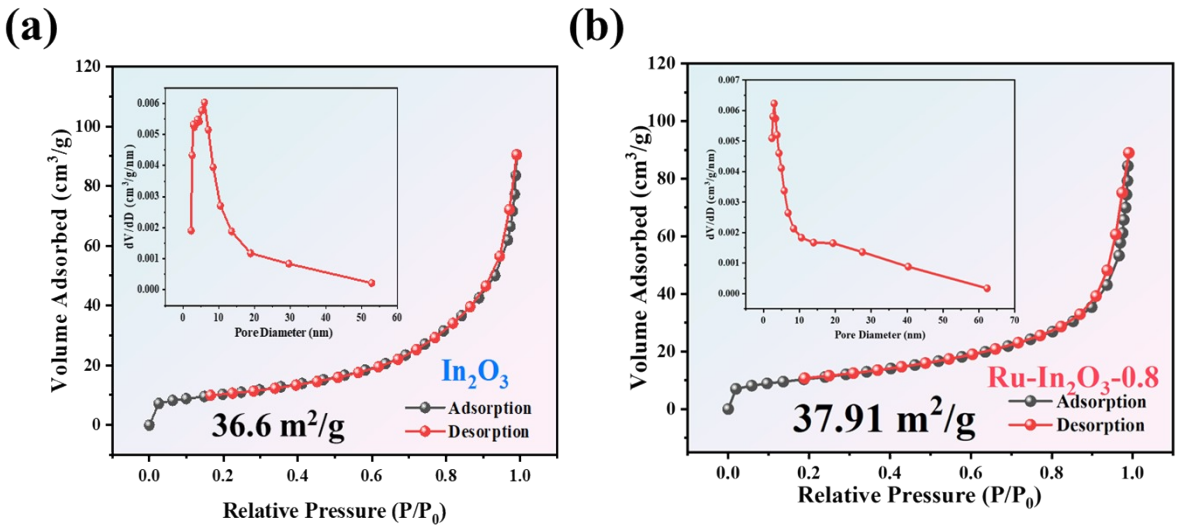

Fig. S3. Nitrogen adsorption-desorption isotherms of In_2O_3 (a) and Ru-In_2O_3-0.8 (b); the inset displays the pore distribution.

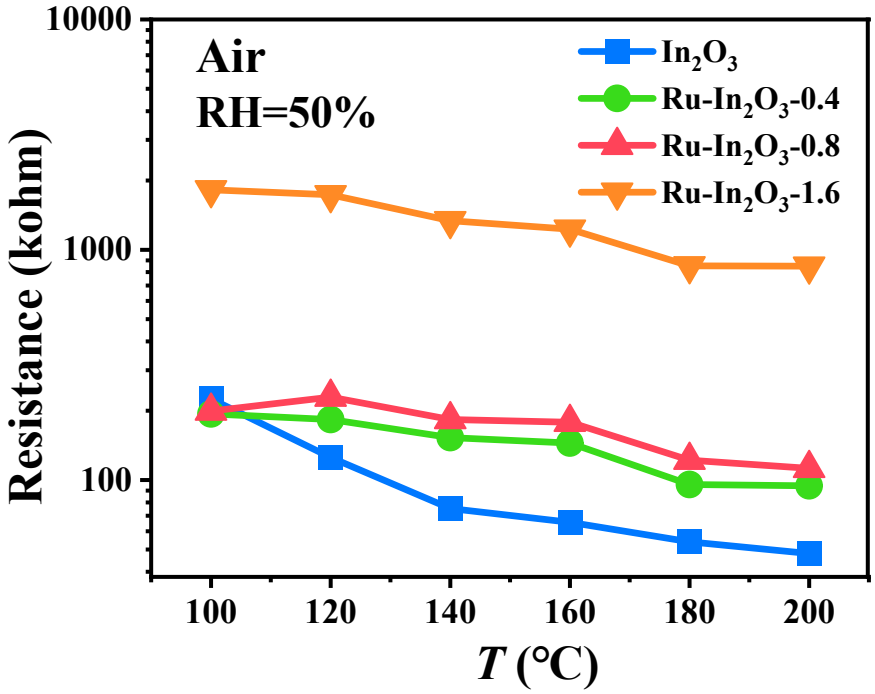

Fig. S4. Resistance values of all sensors at different temperature under 50%RH.

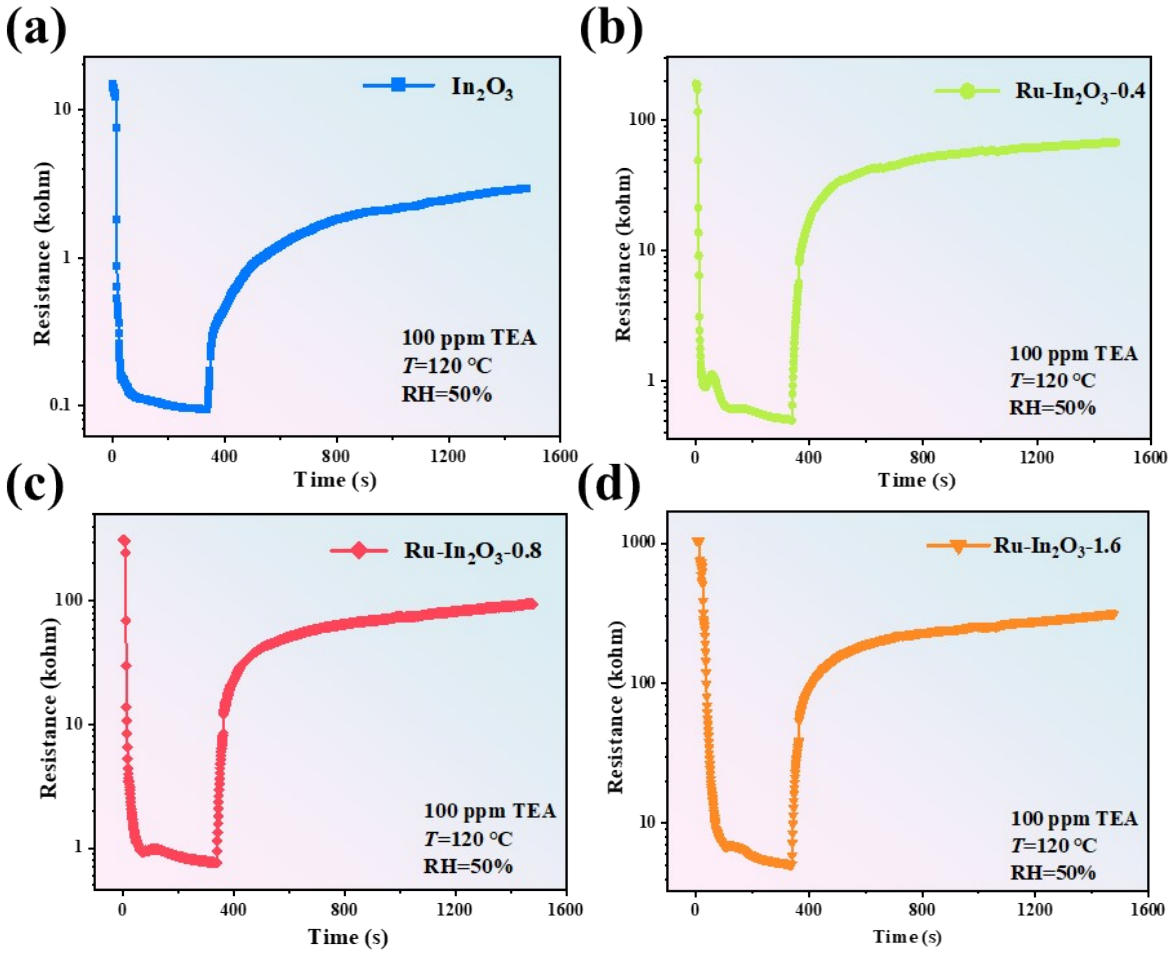

Fig. S5. Resistance curve of (a) In_2O_3, (b) Ru- In_2O_3-0.4, (c) Ru- In_2O_3-0.8 and (d) Ru- In_2O_3-1.6 sensors toward to 100 ppm TEA gas at 120 ℃.

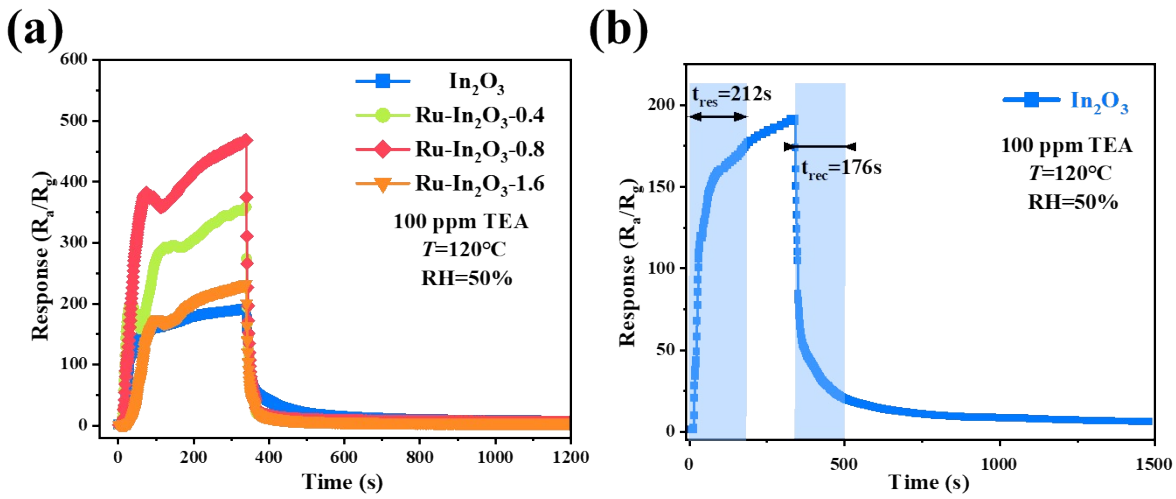

Fig. S6. (a) Response curve of each sensor and (b) Response/recovery time of In_2O_3 sensor to 100 ppm TEA gas at 120 ℃.

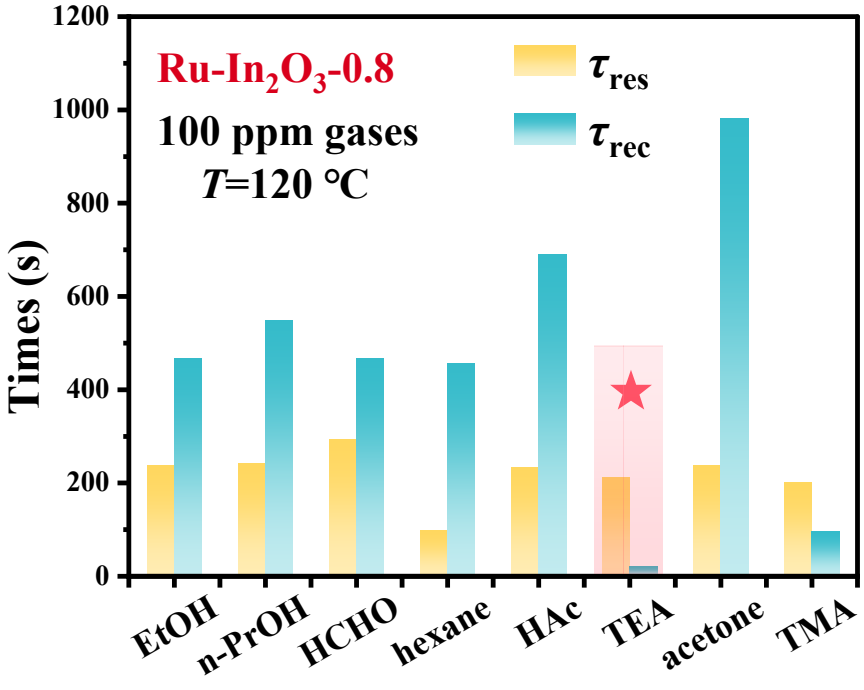

Fig. S7. Response/recovery times of Ru-In_2O_3-0.8 sensor to 100 ppm different gases at 120 ℃ under 50%RH.

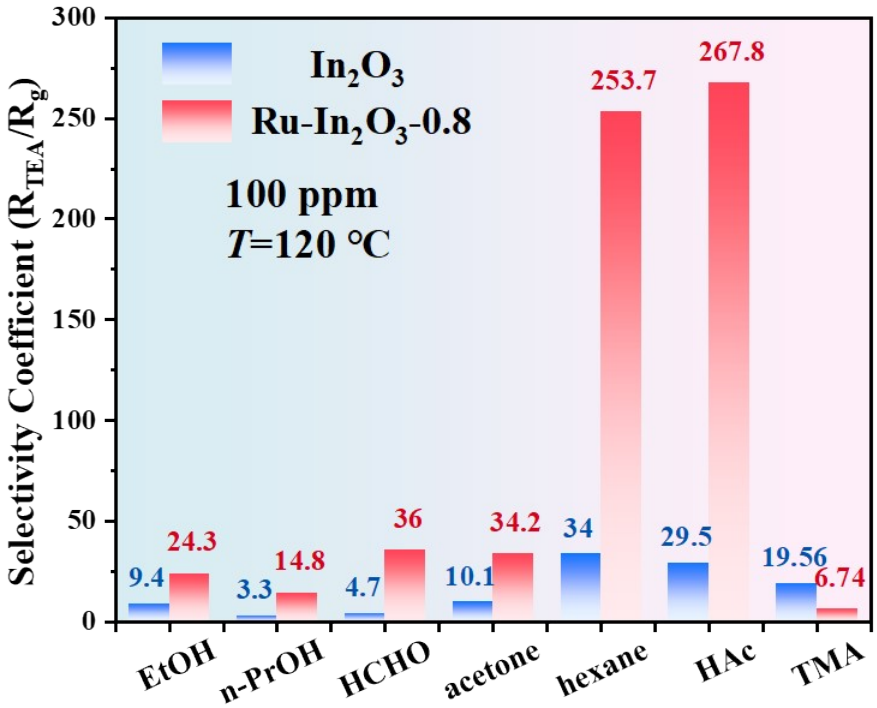

Fig. S8. Selectivity Coefficient toward different gases of In_2O_3 and Ru-In_2O_3-0.8 at 120 °C.

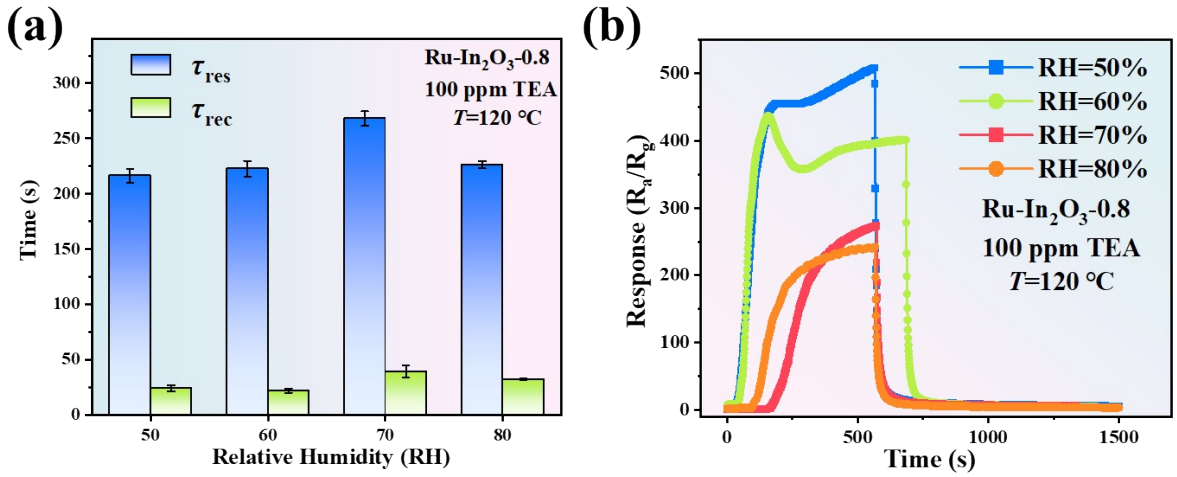

Fig. S9. (a) Response/recovery times and (b) Response curve of Ru-In_2O_3-0.8 to 100 ppm TEA gas at different relative humidity (RH) at optimal operation temperature.

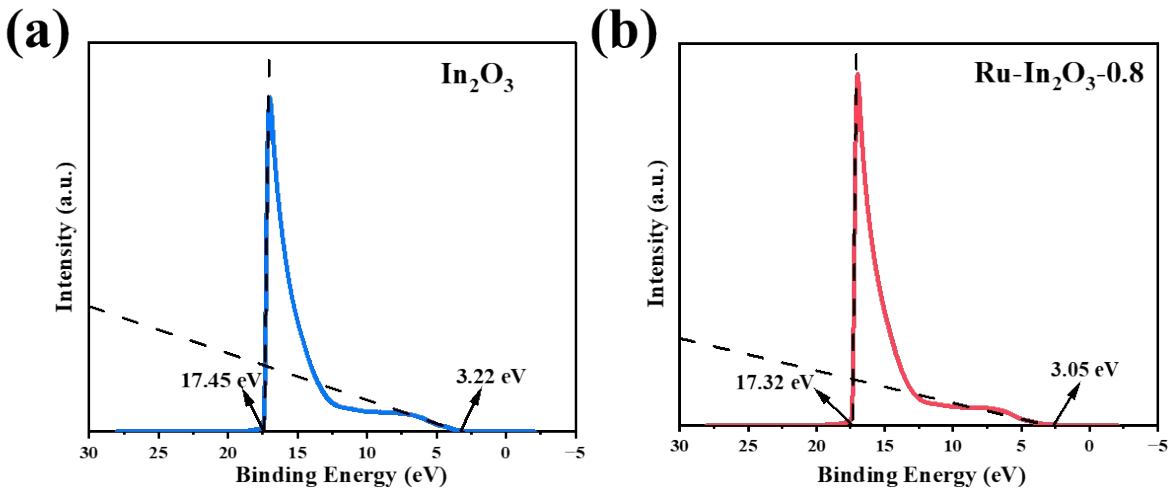

Fig. S10. UPS profiles of In_2O_3 (a) and Ru-In_2O_3-0.8 (b).

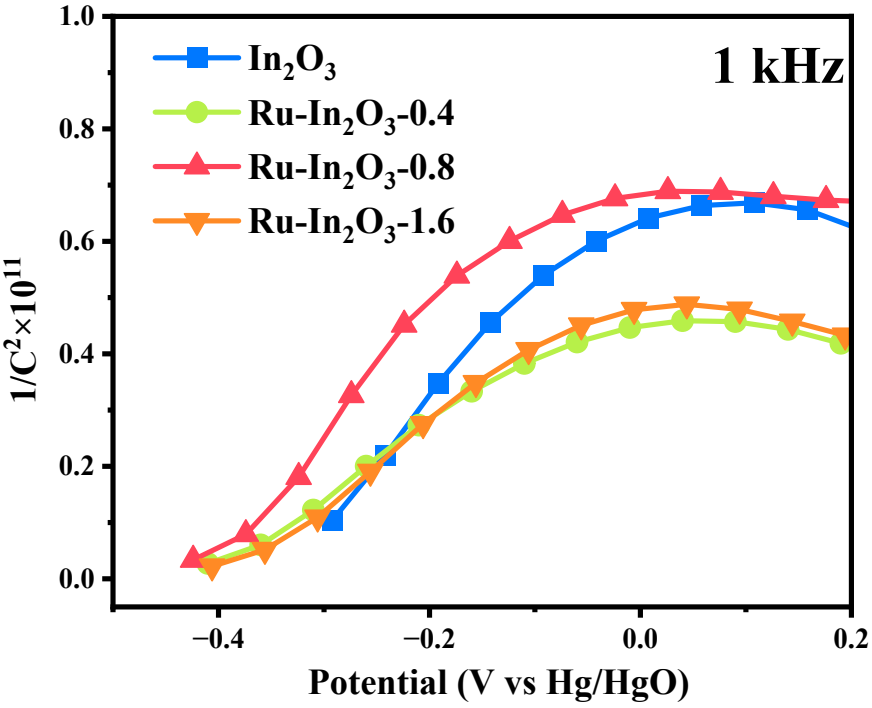

Fig. S11. Mott-Schottky plots of In_2O_3, Ru-In_2O_3-0.4, Ru-In_2O_3-0.8 and Ru-In_2O_3-1.6 microtubes.

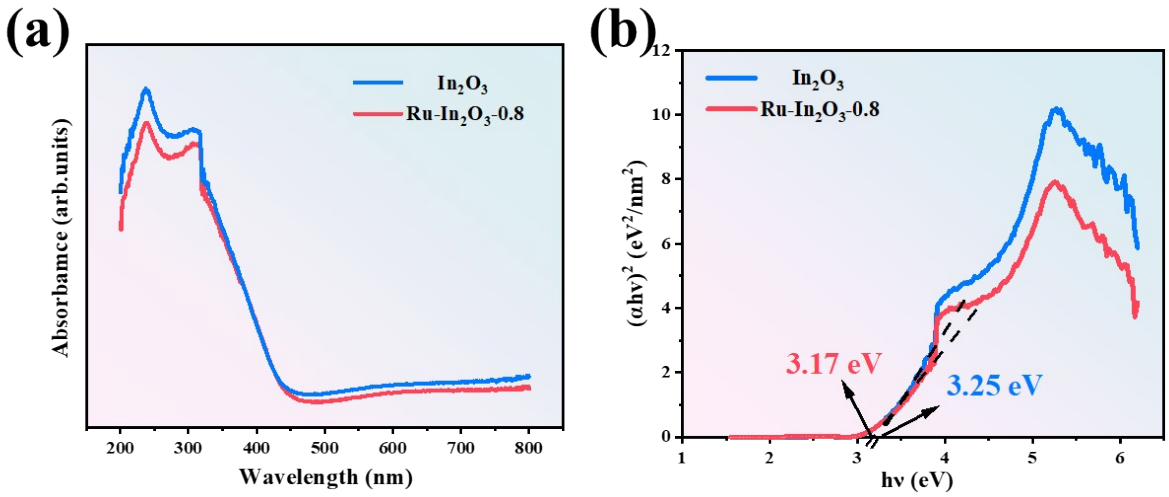

Fig. S12. The UV–visible absorbance spectra of pristine In_2O_3 and Ru-In_2O_3-0.8 samples (a) and the $(\alpha hv)^2$-hv curves of the samples (b).

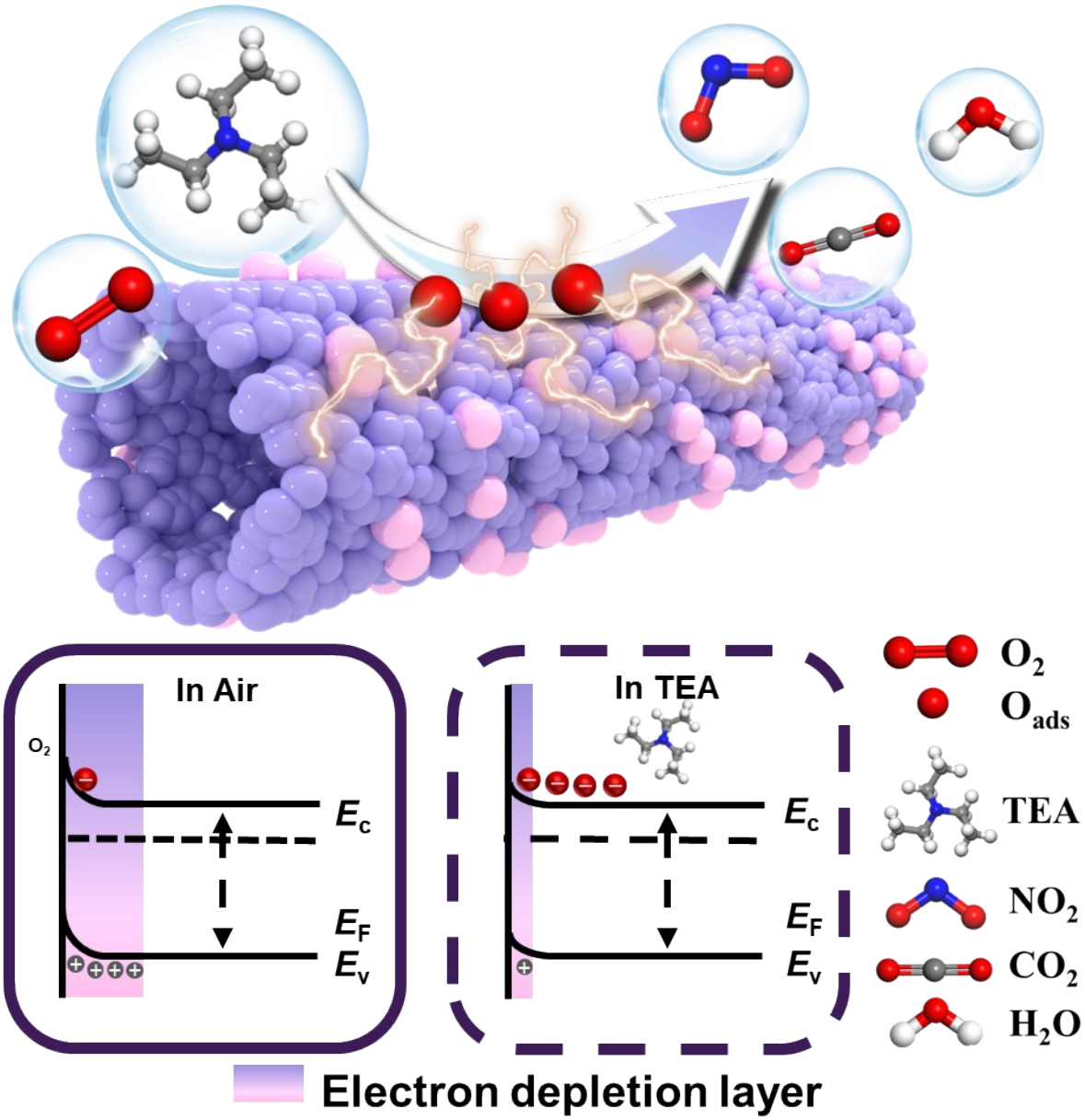

Fig. S13. Schematic of the gas sensing mechanism and the electron depletion layer changes on Ru-In_2O_3-0.8 surface.

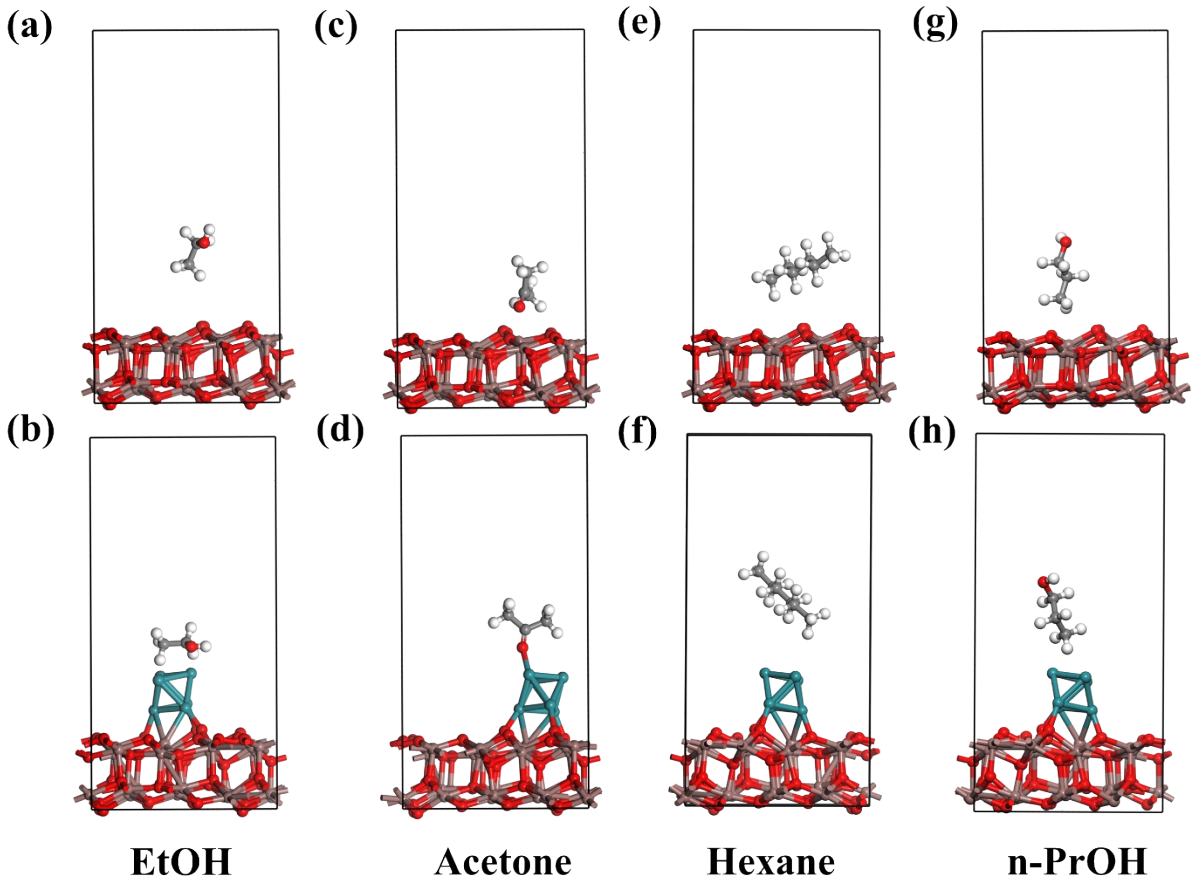

Figure S14. Adsorption models of different gas molecules on In_2O_3 (222) and Ru-In_2O_3 (222) surface.

Shrimp testing condition:

A 100 g sample of fresh shrimp was hermetically sealed in a 500 mL beaker at a room temperature of 15 ℃ and relative humidity of 20%. Subsequently, 25 mL of headspace gas was extracted from the beaker at regular intervals and injected into a 20 L sealed container, and use the smart gas sensor to detect the concentration of TEA gas.

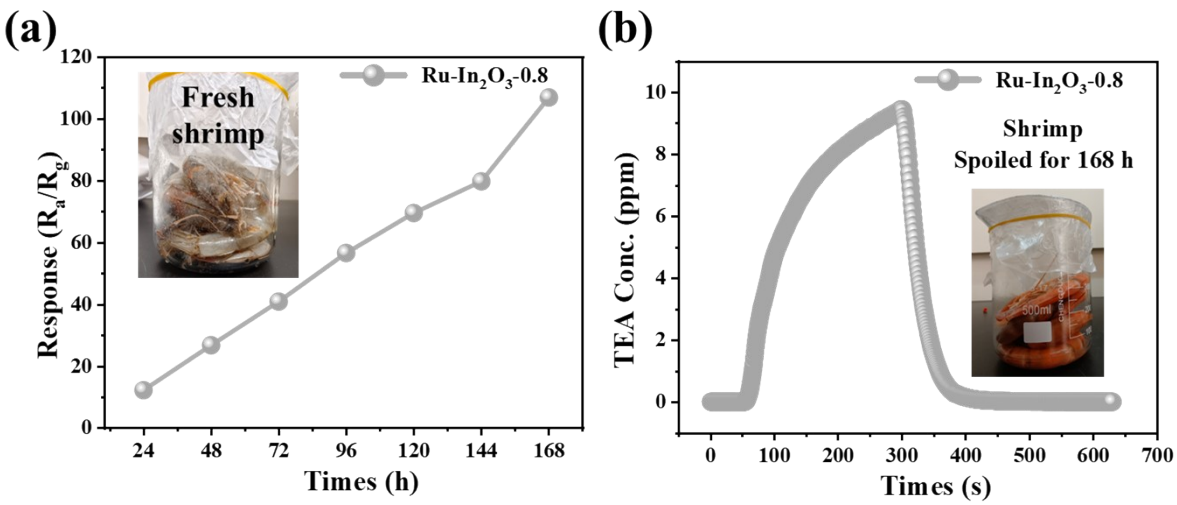

Fig. S15 (a) Response values to the volatile biomarker TEA of shrimps spoiled for different periods at 120 ℃. (b) TEA concentration curve of shrimps spoiled for 168 hours at 120 ℃.

Table S1. The comparison of sensing performance of Ru-In_2O_3-0.8 materials and other previously-reported triethylamine sensing materials.

Materials	Temp. (℃)	Conc. (ppm)	Resp. (R_a/R_g)	τ_{rec} (s)	LOD (ppb)	Year	Ref.
RuCu- In_2O_3 microspheres	240	100	72	20	30.8	2025	[1]
In_2O_3/ErVO4	250	100	50.4	52	1,000	2024	[2]
SnO_2- In_2O_3 nanofibers	200	100	31.9	75	475.71	2025	[3]
In_2O_3@Co_3O_4 nanofibers	120	50	40.5	4	10,000	2025	[4]
Al-doped In_2O_3 nanotubees	120	1	92.8	138	31	2025	[5]
In_2O_3/TiO_2 nanofibers	280	100	131.6	17	13.5	2025	[6]
Ru@Mxene	120	50	24	50	50	2025	[7]
Ru-SnMOF@SnO_2	250	100	688.6	87	1000	2024	[8]
RuO_2-ZnO nanosheets	200	50	85	610	1000	2025	[9]
Ru-In_2O_3-0.8 microtubes	**120**	**100**	**493**	**22**	**11.3**	**2025**	**This work**

Table S2. Adsorption energy of Ru-In_2O_3 (222) and In_2O_3 (222) for different gases.

Adsorption Energy (eV)	TEA (eV)	EtOH (eV)	Acetone (eV)	Hexane (eV)	n-PrOH (eV)
Ru-In_2O_3	-3.95	-0.36	-0.32	-0.43	-0.30
In_2O_3	-0.72	-0.45	-0.65	-1.02	-1.01

The exact procedures used for calculation of LOD.

$$LOD = 3 * \sigma/Slope\#(Equation\ 4)$$

$$\sigma = \sqrt{\frac{\Sigma(y_i - y)^2}{N}}\#(Equation\ 5)$$

Sensor noise is defined as the deviation (y_i - y) of each measured baseline response without target gas (y_i) from the optimal baseline value, y = 1. The corresponding yi values are listed in Table S3, N denotes the total number of these data points and S in the Equation 4 denotes the slope of the linear fit.

σ = 0.034015

LOD = (3*σ)/S = 3*0.034015/8.908 = 0.01134 ppm ≈ 11.3 ppb

Table S3. Baseline measurements without the target gas consisted of 30 data points.

y_i	0.993	1.077	0.980	0.986	0.991	0.998	1.001	0.987
	1.077	1.011	0.999	1.082	1.012	1.019	0.994	1.008
	1.011	1.010	1.070	1.004	0.989	0.991	1.08	0.984
	1.019	1.013	0.986	0.992	1.030	1.011		

1. Z. Zhao, Z. Jin, A. Yousaf, H. Li and L. Wu, TEA gas sensors towards seafood spoilage detection based on RuCu nanoalloys decorated In_2O_3 nanoparticles: Experiment and DFT calculation, *Appl. Surf. Sci.*, 2025, **709**, 163669.
2. X.-B. Li, X. Hu, B. Yang, L.-H. Zheng, Y.-Y. Ren, F.-P. Wang, S. Sun, Y.-J. Wang, D.-N. Liu, H.-H. Xu, D.-W. Chen, W.-Q. Dang, Y.-X. Zhao and F.-R. Jin, Heterostructure engineering of $In_2O_3/ErVO_4$ hairy curd for high-performance TEA gas sensors, *Ceram. Int.*, 2024, **50**, 29590-29602.
3. S. Li, Z. Hu, T. Wang, F. Song, H. Shao, F. Li and X. Dong, Selectivity towards Triethylamine gas detection induced by Janus heterostructure of n-n type SnO_2-In_2O_3 nanofibers, *J. Alloys Compd.*, 2025, **1032**, 181270.
4. Q. Xie, M. Liu, B. Sun and P. Song, Efficient detection of triethylamine by $In_2O_3@Co_3O_4$ core-shell nanofibers synthesized by coaxial electrospinning, *Sens. Actuators, B*, 2025, **439**, 137831.
5. O. Wang, J. Kong, Y. Sun, Y. Tang, H. Wang, B. An, Q. Hu, J. Xu and X. Wang, Improving triethylamine vapor detection capabilities of In_2O_3 via aluminum-mediated isomorphic replacement in the crystalline structure, *Sens. Actuators, B*, 2025, **441**, 137989.
6. J. He, X. Qi, J. Liu, H. Zhang, Z. Wang and S. Duo, Coaxial electrospinning In_2O_3/TiO_2 core-shell nanofibers for enhanced triethylamine sensing, *Sens. Actuators, B*, 2025, DOI: 10.1016/j.snb.2025.138313.
7. P. Zhu and A. Zhu, High performance triethylamine sensor based on Ru nanoparticles decorated 2D-$Ti_3C_2T_x$ MXene nanosheets, *Mater. Lett.*, 2025, **389**, 138379.
8. Z. Liu, Y. Wang, Y. Li, C. Sui, Y. Liu, Y. Liu, Y. Zhao, X. Liang, F. Liu and G. Lu, Bimetallic MOF derived mesoporous structure of Ru doped SnO_2 enable high-sensitivity gas sensors for triethylamine in high humidity, *Sens. Actuators, B*, 2024, **405**, 135275.
9. J. Li, H. Dong, M. Cheng, J. Ge, Y. Wu, H. Lv, X. Zhou, R. Gao, Y. Wang and G.-D. Li, RuO_2-decorated ZnO nanosheets for enhanced triethylamine detection: A promising sensor for fish freshness assessment, *Sens. Actuators, B*, 2025, **443**, 138241.